# 6

# Low Rate High Frequency Data Transmission from Very Remote Sensors

Pau Bergada, Rosa Ma Alsina-Pages, Carles Vilella and Joan Ramon Regué
*La Salle - Universitat Ramon Llull*
*Spain*

## 1. Introduction

This chapter deals with the difficulties of transmitting data gathered from sensors placed in very remote areas where energy supplies are scarce. The data link is established by means of the ionosphere, a layer of the upper atmosphere that is ionized by solar radiation. Communications through the ionosphere have persisted, although the use of artificial repeaters, such as satellites, has provided more reliable communication. In spite of being random, noisy and susceptible to interference, ionospheric transmission still has favorable characteristics (e.g. low cost equipment, worldwide coverage, invulnerability, etc.) that appeal to current communications engineering.

The Research Group in Electromagnetism and Communications (GRECO) from La Salle - Universitat Ramon Llull (Spain) is investigating techniques for the improvement of remote sensing and skywave digital communications. The GRECO has focused its attention on the link between Antarctica and Spain. The main objectives of this study are: to implement a long-haul oblique ionospheric sounder and to transmit data from sensors located at the Spanish Antarctic Station (SAS) Juan Carlos I to Spain.

The SAS is located on Livingston Island (62.7 °S, 299.6 °E; geomagnetic latitude 52.6 °S) in the South Shetlands archipelago. Spanish research is focused on the study of the biological and geological environment, and also the physical geography. Many of the research activities undertaken at the SAS collect data on temperature, position, magnetic field, height, etc. which is temporarily stored in data loggers on-site. Part of this data is then transmitted to research laboratories in Spain. Even though the SAS is only manned during the austral summer, data collection never stops. While the station is left unmanned, the sets of data are stored in memory devices, and are not downloaded until the next Antarctic season. The information that has to be analyzed in almost real-time is transmitted to Spain through a satellite link. The skywave digital communication system, presented here, is intended to transmit the information from the Antarctic sensors as a backup, or even as an alternative to the satellite, without depending on other entities for support or funding.

Antarctica is a continent of great scientific interest in terms of remote sensing experiments related to physics and geology. Due to the peculiarities of Antarctica, some of these experiments cannot be conducted anywhere else on the Earth and this fact might oblige the

researchers to transmit gathered data to laboratories placed on other continents for intensive study. Because of the remoteness of the transmitter placed at the SAS, the system suffers from power restrictions mainly during austral winter. Therefore, maintaining the radio link, even at a reduced throughput, is a challenge. One possible solution to increase data rate, with minimal power, is to improve the spectral efficiency of the physical layer of the radio link while maintaining acceptable performance. The outcomes and conclusions of this research work may be extrapolated to other environments where communication is scarcely possible due to economic or coverage problems. Therefore, the solutions presented in this study may be adopted in other situations, such as communications in developing countries or in any other remote area.

### 1.1 Remote sensors at the SAS

In this section we describe the main sensors located at the SAS, including a geomagnetic sensor, a vertical incidence ionosonde, an oblique incidence ionosonde and a Global Navigation Satellite System (GNSS) receiver. They have all been deployed in the premises of the SAS by engineers of the GRECO and scientist of the Observatori de l'Ebre. The geomagnetic sensor, the vertical incidence ionosonde and the GNSS receiver are commercial solutions. The oblique incidence ionosonde, used to sound the ionospheric channel between Antarctica and Spain, was developed by the GRECO in the framework of this research work.

#### 1.1.1 Geomagnetic sensor

Ground-based geomagnetic observatories provide a time series of accurate measurements of the natural magnetic field vector in a particular location on the Earth's surface. This data is used for several scientific and practical purposes, including the synthesis and updates of global magnetic field models, the study of the solar-terrestrial relationships and the Earth's space environment, and support for other types of geophysical studies.

Once the raw observatory data is processed, it is sent to the World Data Centers, where the worldwide scientific community can access them. International Real-time Magnetic Observatory Network (INTERMAGNET) provides means to access the data by an almost real-time satellite link. The data is packed, sent to the geostationary satellites, and collected by Geomagnetic Information Nodes (GINs), where the information can be accessed freely. However, experience has shown that the satellite link is not 100% reliable, and it is preferable to have alternative means to retrieve the geomagnetic data.

There are three main reasons for designing a transmission backup system by skywave. Firstly, visibility problems appear when trying to reach geostationary satellites from polar latitudes. Secondly, end-to-end reliability can be increased by transmitting each frame repeatedly throughout the day. And finally, the ionospheric channel is freely accessed anywhere, whereas satellite communications have operational costs.

#### 1.1.2 Ionosonde: vertical incidence soundings of the ionosphere

A vertical incidence ionospheric sounder (VIS) (Zuccheretti et al., 2003) was installed in order to have a sensor providing ionospheric monitoring in this remote region. This ionosonde is also being used to provide information for the High Frequency (HF) radio link employed

for data transmission from the SAS to Spain. Data provided by the VIS is used to conduct ionospheric research, mainly to characterize the climatology of the ionospheric characteristics and to investigate the ionospheric effects caused during geomagnetically disturbed periods (see (Solé et al., 2006) and (Vilella et al., 2009)).

#### 1.1.3 Oblique ionosonde

The oblique ionosonde monitors various parameters to model the HF radiolink between the SAS and Spain (Vilella et al., 2008). These parameters include link availability, power delay profile and frequency dispersion of the channel. The sounder includes a transmitter, placed on the premises of the SAS and a receiver deployed in Spain. The main drawback of the oblique sounder is the difficulty in establishing the ionospheric link. Firstly, the long distance of the link (12700 km) requires four hops to reach the receiver. And secondly, the transmitted signal has to cross the equator and four different time zones.

#### 1.1.4 Global Navigation Satellite Systems

The ionosphere study can be approximated from several points of view. Vertical incidence soundings provide accurate information about electron density profiles below the peak electron density. However, when using this technique the electron profile must be extrapolated from the peak point to the upper limit of the ionosphere. Moreover, the low density of vertical ionosondes, especially in oceans and remote areas, is a serious impairment.

GNSS receivers constitute a high temporal and spatial resolution sounding network which despite gaps over oceans and remote regions, can be used to study fast perturbations affecting local regions, such as Travelling Ionospheric Disturbances and scintillations, or wider regions such as solar flares. Data gathered from GNSS receivers can provide information about the Total Electron Content (TEC) between receivers and satellites by means of proper tomographic modeling approaches. Spatial and temporal variations of the main ionospheric events can be monitored by means of GNSS receivers, especially those placed in the Antarctic Region, which is considered the entrance point of many ionospheric disturbances coming from Solar events. Furthermore, TEC reaches its highest variability peaks in the Antarctica area.

### 1.2 Data transmission

This chapter will study, analyze and experimentally verify a possible candidate for the physical layer of a long-haul ionospheric data link, focusing on the case SAS-Spain. Preliminary studies of data transmission feasibility over this link were already performed in (Deumal et al., 2006) and (Bergada et al., 2009), with encouraging results.

The first application of this link is the transmission of data generated by a geomagnetic sensor installed at the SAS. Future applications may include sending information of another nature such as temperature, glacier movements, seismic activity, etc.

The minimum requirements regarding the geomagnetic sensor data transmissions from the SAS to Spain are:

- The system should support a data throughput of 5120 bits per hour.
- The maximum delivery delay of the data should not exceed 24 hours.

### 1.2.1 Constraints

The extreme conditions prevailing at the SAS impose a number of restrictions that affect the transmission system. We highlight the following ones:

- The transmission power should be minimal. It is noted that the SAS is inhabited only during the austral summer, approximately from November to March. During this period there is no limitation regarding the maximum power consumption. However, the transmission system is designed to continue operating during the austral winter, when energy is obtained entirely from batteries powered by wind generators and solar panels. Hence the power amplifier is set to a maximum of only 250 watts.
- Environmental regulations applicable at the site advise against the installation of large structures that would be needed to install certain types of directive antennas.

### 1.2.2 Approach

This section justifies the need for a new data communication system adapted to the requirements of the project and presents the main ideas of this proposal. Firstly, we review the mechanisms that exist worldwide regarding the regulation of occupation of the radio spectrum. Then we review the features of current standards of HF data communications and discuss the non-suitability of these to the requirements of the project.

The International Telecommunication Union (ITU) is responsible for regulating the use of radio spectrum. From the point of view of frequency allocation, it has divided the world into three regions. Broadly speaking, region 1 comprises Europe and Africa, Asia and Oceania constitute region 2 and North and South America region 3.

In each region, the ITU recommends the allocation of each frequency band to one or several services. When multiple services are attributed to the same frequency band in the same region, these fall into two categories: primary or secondary. The ones that are classified as secondary services can not cause interference with the primary services and can not claim protection from interference from the primary services; however, they can demand protection from interference from other secondary services attributed afterwards.

Given these considerations, we propose a system transmission with the following guidelines:

- It can not cause harmful interference to any other service stations (primary or secondary).
- It can not claim protection from interference from other services.

To meet these requirements, we propose a system with the following characteristics:

- Reduced transmission power (accordingly with the consumption constrains).
- Low power spectral density.
- Robustness to interference.
- Burst transmissions (few seconds).
- Sporadic communications.

Moreover, given the ionospheric channel measures described in (Vilella et al., 2008) the following additional features are required:

- Robustness against noise (possibility of working with negative signal to noise ratio).
- Robustness against time and frequency dispersive channels.

### 1.2.3 HF communication standards

In this section we briefly review the current communication standards for HF and we justify its non-suitability for the purposes of this project.

Due to the proliferation of modems in the field of HF communications, interoperability between equipment from different manufacturers became a problem (NTIA, 1998). Hence the need to standardize communication protocols. Worldwide, there are three organizations proposing standards regarding HF communications: $(i)$ the U.S. Department of Defense proposes the Military Standards (MIL-STD-188-110A, 1991; MIL-STD-188-110B, 2000; MIL-STD-188-141A, 1991), $(ii)$ the Institute for Telecommunications Science (ITS), which depends on the U.S. Department of Commerce, writes the Federal Standard (FED-STD) and $(iii)$ NATO proposes the Standardization Agreements (STANAG-4406, 1999; STANAG-5066, 2000).

Regarding the interests of this work it is noted that:

- The standard modes are designed for primary or secondary services. Therefore:
  - The bandwidth of the channels is standardized (3 kHz or multiples). Interference reduction, i.e. minimize the output power spectral density, with other transmitting systems is not considered.
  - No modes are considered based on short sporadic burst transfers to reduce interference with other users.
  - There are anti-jamming techniques (see MIL-STD-188-148) for additional application on a appropriate communication standard, but the proposals are not based on intrinsically robust to interference modulations.
- Robust configurations require a minimum signal to noise ratio (SNR) of 0 dB at 3 kHz bandwidth, which is not common in this link under the specified conditions of transmitted power and antennas (Vilella et al., 2008).

We conclude that the configurations proposed by current standards do not meet the desirable characteristics for the type of communication that is required in this work, and consequently, a new proposal should be suggested. In this chapter, we study a number of alternatives based on the use of Direct Sequence Spread Spectrum (DS-SS) techniques in order to cope with the impairments of the channel, the environment and other services.

## 2. Data transmission with Direct Sequence Spread Spectrum techniques

Spread Spectrum (SS) techniques are described by (Pickholtz et al., 1982) as a kind of transmission in which signal occupies a greater bandwidth than the necessary bandwidth to send the information; bandwidth spreading is achieved by an independent data source, and a synchronized code in the receiver to despread and retrieve data.

SS began to be developed especially for military purposes in the mid twentieth century and has continued in the forefront of research to present, which is, nowadays, a key point for the 3G mobile cellular systems (Third Generation Partnership Project, 1999) and wireless systems transmitting in free bands (IEEE802.11, 2007).

In the field of HF communications new techniques have always been slowly introduced due to a widespread sense that reliable communications were not feasible in this frequency band, while improvements of its implementation would be irrelevant. However, SS techniques have been suggested several times as suitable for the lower band of frequencies (i.e. LF, MF and, by extension, HF) (see (Enge & Sarwate, 1987)), since the intrinsic characteristics of SS systems to cope with multipath and interference (typical ionospheric channel characteristics).

There are three types of spread spectrum systems (Peterson et al., 1995): Direct Sequence, Frequency Hopping and hybrid systems composed by a mixture of both. In this study we will focus on Direct Sequence schemes.

DS-SS systems spread the spectrum by multiplying the information data by a spreading sequence. Consider the following model (Proakis, 1995):

$$s_{ss}(t) = \sum_{i=0}^{N_s-1} d_i c(t - iT_s),\ c(t) = \sum_{l=0}^{L-1} c_l p(t - lT_c), \tag{1}$$

where $d_i$ denotes the $i_{th}$ symbol, of length $T_s$, of a modulated signal:

$$\overline{d} = \{d_0, d_1, ..., d_{N_s-1}\} \tag{2}$$

and $c_l$ are the chips [1], of length $T_c$, of a spreading sequence of length $L$:

$$\overline{c} = \{c_0, c_1, ..., c_{L-1}\} \tag{3}$$

and $p(t)$ is a pulse shaping defined as

$$p(t) = \begin{cases} 1, t \in [0, T_c) \\ 0 \Rightarrow \text{otherwise} \end{cases} \tag{4}$$

In addition, it holds that $LT_c = T_s$ and thus if the base band signal is formed by the symbols $d_i$ and occupies a bandwidth of $\frac{1}{T_s}$ the spread spectrum signal $s_{ss}(t)$ occupies a bandwidth of $\frac{1}{T_c} = L\frac{1}{T_s}$.

The spreading sequence $\overline{c}$ should have good properties of autocorrelation and cross-correlation in order to ease the detection and synchronization at the receiver side.

Some of the main advantages of a system based on DS-SS are: $(i)$ jamming and interference robustness, $(ii)$ privacy, $(iii)$ ability to use Code Division Multiple Access (CDMA) and $(iv)$ robustness against multipath and time variant channels. On the other hand, the drawbacks of this technique are: $(i)$ bandwidth inefficiency and $(ii)$ receiver complexity: chip-level synchronization, symbol despreading (DS-SS signaling) and channel estimation and detection (RAKE receiver) (Viterbi, 1995).

Throughout the following sections we will discuss the most important considerations that justify the choice of DS-SS; as well as the technical basis to design the data modem for the ionospheric link between the SAS and Spain.

[1] The bits of a spreading sequence are called chips

### 2.1 Robustness against interference

Ionospheric communications have global coverage range. Consequently, any system operating in a given area might potentially interfere with other remote systems operating at the same frequency band. Hence the transmission system proposed in this work might be interfered with primary or secondary services that are assigned the same frequency band. For these reasons it is appropriate to review the characteristics of DS-SS regarding robustness against interference.

Let a DS-SS based system that transmits $R_b$ bits per second in a bandwidth $B_{ss}$ ($B_{ss} \gg R_b$) in the presence of additive white Gaussian noise $z(t)$ with power spectral density $N_o$ $[W/Hz]$ and narrowband interference $i(t)$ with power $P_i$. At the receiver side:

$$r_{ss}(t) = s_{ss}(t) + i(t) + z(t). \tag{5}$$

Then (Pickholtz et al., 1982),

$$\left(\frac{E_b}{N_o}\right)_{z(t),i(t)} = \frac{P}{P_n}\frac{B_{ss}}{R_b}\frac{P_n}{P_n + P_i} = \frac{P}{P_n}\frac{B_{ss}}{R_b}\frac{N_0}{N_0 + \frac{P_i}{B_{ss}}}, \tag{6}$$

where $P_n = B_{ss}N_o$ is the noise power within the transmission bandwidth and $P = E_b R_b$ is the signal power. We can deduce from Equation 6 that we can reduce the effect of interfering signals by increasing $B_{ss}$. In other words, as $B_{ss} = L \cdot R_b$, the larger the spreading factor the lower the degradation due to interfering signals. The quotient $\frac{B_{ss}}{R_b}$ is called the process gain $G_p$ and is a measure of the robustness of a spread spectrum system against interference. In DS-SS systems the processing gain coincides with the spreading sequence length $(L)$.

It is noted that when $B_{ss}$ increases $\left(\frac{E_b}{N_o}\right)\Big|_{z(t)}$ does not change because $P_n = N_o B_{ss}$ increases in the same proportion, whereas an increase of $B_{ss}$ implies an equivalent improvement of $\left(\frac{Eb}{N_o}\right)\Big|_{i(t)}$, as $P_i$ is unchanged. To summarize, the use of spread spectrum provides improvement regarding narrowband interfering signals whereas no improvement over noise is achieved.

Feasibility studies of DS-SS systems with different types of interference can be found in the literature. See, for instance, (Schilling et al., 1980) when the interference is a narrowband signal and (Milstein, 1988) for multiple interfering signals.

### 2.2 Robustness against multipath channels

According to the analysis described in (Vilella et al., 2008), the ionospheric channel established between the SAS and Spain shows a maximum multipath delay spread ($\tau_{max}$) that varies, depending on time and frequency, between 0.5 ms and 2.5 ms. Therefore, the coherence bandwidth of the channel, which can be considered as approximately the inverse of the maximum multipath delay spread (Proakis, 1995), can be narrower than 400 Hz. In case of transmitting with a wider bandwidth the channel would be frequency selective and distortion due to multipath would arise. Below, the properties of DS-SS against multipath are discussed.

Let a DS-SS based system with bandwidth $B_{ss}$ in a channel with coherence bandwidth $W_c \sim \frac{1}{\tau_{max}} \ll B_{ss}$. If symbol time $T_s \gg \tau_{max}$ intersymbol interference due to multipath can be

neglected. Moreover, if $T_s \ll \frac{1}{v_{max}}$ (where $v_{max}$ denotes the maximum Doppler spread) the channel is almost invariant during a symbol time. Under these conditions it can be shown that (Proakis, 1995):

$$r_{ss}^{(k)}(t) = \sum_{n=1}^{N} h\left(\frac{n}{B_{ss}}\right) s_{ss}^{(k)}\left(t - \frac{n}{B_{ss}}\right) + z(t), \tag{7}$$

where $h\left(\frac{n}{B_{ss}}\right)$ denotes a coefficient of the equivalent low-pass of the channel impulse response, $s_{ss}(t)$ corresponds to the base band spread signal defined in Equation 1, $^{(k)}$ denotes the contribution due to symbol $k$, $N = \tau_{max} B_{ss}$ is the number of non zero channel taps (since $s_{ss}(t)$ has a limited bandwidth of $B_{ss}$) and $z(t)$ is additive white Gaussian noise. In consequence, the signal reception is formed by delayed replicas of the transmitted signal. Then, we substitute Equation 1 in Equation 7 and apply an array of correlators to correlate the received signal with $N$ copies of the spreading sequence $\overline{c}$ (each of them delayed a chip time). Let $\overline{c}$ be a sequence with good properties of circular autocorrelation:

$$\rho(m) = \sum_{l=1}^{L} c_l c_{l+m} \begin{cases} 1, \ m = 0 \\ 0 \Rightarrow \text{otherwise} \end{cases} \tag{8}$$

The output $U_m$ of each correlator can be expressed as:

$$U_m = d_k h\left(\frac{m}{B_{ss}}\right) + \int_0^{T_s} c(t) z(t + \frac{m}{B_{ss}})\, dt, \ m \in [0, N-1]. \tag{9}$$

Therefore, at the output of each correlator we obtain each transmitted symbol ($d_k$) multiplied by a channel coefficient $h\left(\frac{m}{B_{ss}}\right)$ plus a noise term. Hence, the use of DS-SS can take advantage of different replicas of the signal if correctly combined. The most general linear combination is the criterion of Maximal Ratio Combining that chooses the coefficients that maximize instantaneous SNR (Peterson et al., 1995). To properly apply this method it is mandatory to know the coefficients of the channel. Alternatively, the outputs of the correlators can be equally weighed (Equal Gain Combining), thus simplifying the receiver at the expense of worse performance.

### 2.3 Transmission with low spectral density power

One of the requirements of the proposed transmission system consists in causing minimal interference with primary and secondary services. For this purpose we propose alternatives to minimize power spectral density. We should note that as process gain increases, DS-SS techniques enable transmission with arbitrarily low power density. Suppose the transmission of a data stream $\overline{d}$ using a bandwidth $B_d$ and power $P$. Then the average power spectral density is $D = \frac{P}{B_d} \left[\frac{W}{Hz}\right]$. Under the same conditions of power consider the transmission of the same data stream with DS-SS ($s_{ss}(t)$) by means of a spreading sequence $c(t)$ of length $L$. Then, the spectral occupancy of $s_{ss}(t)$ will be at least $L \cdot B_d$ and the average power spectral density will be $D_{ss} = \frac{P}{L \cdot B_d} \left[\frac{W}{Hz}\right]$.

Therefore, the use of DS-SS involves an average reduction of power spectral density by a factor equal to the process gain $G_p = L$. Then, the spectral occupancy proportionally increases; however, it is not an inconvenience in this case since there is no limitation in this regard.

### 2.4 Flexibility regarding spectral efficiency

The signal model expressed by Equation 1 is able to transmit $k = \log_2 K$ bits $(b_0^{(0)} \dots b_{k-1}^{(0)})$ modulated in $d_i$ during a period $T_s$ ($K$ is the number of possible modulation symbols in $\overline{d}$ and $k$ is the corresponding number of bits per symbol).

The spectral efficiency ($C_{ss} = k/(T_s \cdot B_{ss})$), expressed in $[bits/s/Hz]$ and defined as the ratio between bit-rate and transmission bandwidth, is $G_p$ times lower than the non spreading system.

There are several alternatives to increase spectral efficiency without decreasing process gain (and hence, robustness to interference) at the expense of increasing computational cost of the receiver. In the following sections we describe two of them: DS-SS M-ary signaling and quadriphase spreading. We briefly present the signal model, a study of the probability of error and we note the spectral efficiency of each of them.

#### 2.4.1 DS-SS M-ary signaling

Let a set of $M$ spreading sequences $Q = \left\{\overline{c}^{(1)}, \overline{c}^{(2)}, \dots, \overline{c}^{(M)}\right\}$ that satisfy a certain correlation relationship (orthogonal or nearly orthogonal according to Equation 8). Suppose that a certain sequence $v$ from the previous set ($v \in [1, M]$) is transmitted depending on the value of $m = \log_2(M)$ bits of information. Then

$$s_{ss}(t) = \sum_{i=0}^{N_s-1} d_i \sum_{l=0}^{L-1} c_l^{(v)} p(t - iT_s - lT_C) = \sum_{i=0}^{N_s-1} d_i c^{(v)}(t). \tag{10}$$

This technique is called DS-SS M-ary signaling (see, for example, (Enge & Sarwate, 1987) for orthogonal sequences). On the receiver side, the optimum demodulator correlates the received signal with a replica of each of the $M$ possible sequences belonging to the set $Q$. A noncoherent detector will make a decision based on the computation of the maximum likelihood of the $M$ envelopes at the output of each correlator. The probability $P_s$ of detecting an incorrect sequence in the presence of only additive white noise is given by (Proakis, 1995):

$$P_s = \sum_{p=1}^{M-1} (-1)^{p+1} \left(\frac{M-1}{p}\right) \frac{1}{p+1} e^{-\frac{p}{p+1}(m+k)\frac{E_b}{N_o}}. \tag{11}$$

The probability $P_1$ of making an error in the demodulation of coded bits transmitted in a certain sequence can be computed from the following expression (Proakis, 1995):

$$P_1 = \frac{2^{m-1}}{2^m - 1} P_s. \tag{12}$$

Once the sequence is detected we proceed to compute the probability $P_2$ of making an error in the demodulation of the coded bits in $\overline{d}$:

$$P_2 = \frac{1}{2} P_s + (1 - P_s)\, Q\left(\sqrt{\frac{2}{k}\left(\frac{E_b}{N_o}\right)'}\right), \tag{13}$$

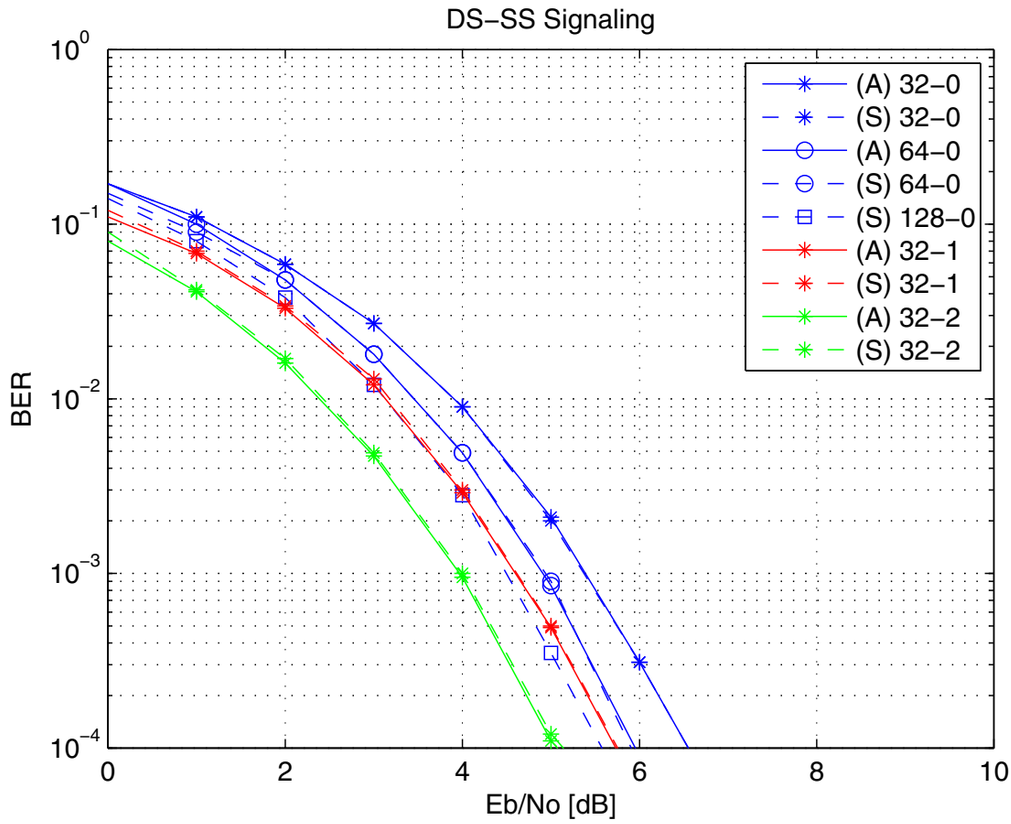


Fig. 1. Probability of error versus SNR per bit using DS-SS M-ary signaling for various values of $M$ (32, 64, 128) and $k$ ($k = 0$ : no modulation, $k = 1$: BPSK, $k = 2$: QPSK). Probability is analytically (A) computed and derived from algorithm simulations (S)

where $\left(\frac{E_b}{N_o}\right)' = \left(\frac{E_b}{N_o}\right)(m+k)$. Finally, the joint probability $P_b$ of bit error considering the contribution of both mechanisms is:

$$P_b = \frac{m \cdot P_1 + k \cdot P_2}{m+k}. \tag{14}$$

Figure 1 shows that the higher the $M$, the lower the SNR per bit required to obtain a certain BER. It can be explained by the fact that $L$ increases as $M$ (in a DS-SS system) and so does the process gain. It can be shown that the minimum SNR per bit required to obtain an arbitrarily small BER when $M \to \infty$ is -1.6 dB. Figure 1 also shows that the larger the $k$, the smaller the SNR per bit required to achieve a given BER. This apparent contradiction can be derived from the following two arguments: (*i*) for a given bit-rate, a high value of $k$ enables the reduction of transmission bandwidth (and thus reduction of noise) and hence, improve the probability of finding the transmitted sequence (Equation 13). (*ii*) The probability $P_b$ of total error (Equation 14) is a balance between $P_1$ and $P_2$. The second term in $P_2$ (Equation 13) derives from the probability of error in demodulating the bits in $\overline{d}$ once the sequence is successfully detected. So, if this term is lower than both the first term in Equation 13 and $P_1$ (Equation 12) the use of any kind of modulation will not result in significant degradation in $P_b$.

In a symbol time $T_s$ we send $k+m$ bits ($b_0^{(1)} \cdots b_{k-1}^{(1)} b_0^{(1)} \cdots b_{m-1}^{(1)}$), where $k$ corresponds to the bits modulated with $\overline{d}$ and $m$ corresponds to the bits used in the choice of the spreading sequence. Consequently, the spectral efficiency is:

$$C = \frac{k+m}{G_p} = C_{ss} + \frac{m}{G_p} = C_{ss} + \frac{\log_2 M}{G_p}. \tag{15}$$

Therefore, the larger the $M$ the lower the BER for a given SNR per bit and the greater the spectral efficiency at the expense of greater computational cost of the receiver. In addition, the larger the number of bits per symbol the better the BER for a given SNR per bit and the lower the computational cost of the receiver.

#### 2.4.2 DS-SS M-ary signaling + Quadriphase

Another alternative is to divide the set of $M$ sequences into two subsets: $Q_r = \{\overline{c}^{(1)}, \cdots, \overline{c}^{(M/2)}\}$ on one side and $Q_i = \{\overline{c}^{(M/2+1)}, \cdots, \overline{c}^{(M)}\}$ on the other side. Then, apply DS-SS M-ary signaling on both the real and the imaginary part of $\overline{d}$. Thus,

$$s_{ss}(t) = \sum_{i=0}^{N_s-1} \left( \Re\{d_i\} c^{(v_1)}(t) + j \cdot \Im\{d_i\} c^{(v_2)}(t) \right), \; v_1 \in [1, M/2], v_2 \in [M/2+1, M]. \tag{16}$$

This variant is called quadriphase chip spreading and permits us to send $M = 2\log_2(M/2)$ bits per symbol by choosing a sequence from each of the two sets (plus $k$ additional bits per symbol encoded in the modulation of $d_i$).

At the receiver side, the demodulator correlates the received signal with a replica of each of the $M$ possible sequences. The detector will decide on the envelopes computed at the output of correlators corresponding to the sequences of the subset $Q_r$ and a similar decision on the subset $Q_i$. The probability of incorrectly detecting a sequence from both the set $Q_r$ and $Q_i$ in the presence of only additive white Gaussian noise is:

$$P_s = \sum_{p=1}^{M/2-1} (-1)^{p+1} \binom{M/2-1}{p} \frac{1}{p+1} e^{-\frac{p}{p+1}\left(\frac{m+k}{2}\right)\frac{E_b}{N_o}}. \tag{17}$$

It is worth noting that the factor $1/2$ multiplying $\frac{E_b}{N_o}$ comes from considering that the symbol energy is equally distributed between real and imaginary parts (see Equation 16). The probability $P_1$ of incorrectly demodulating the bits coded in a sequence that belongs to the subset $Q_r$ or $Q_i$ can be obtained by applying an equation analogous to Equation 12:

$$P_1 = \frac{2^{(m/2)-1}}{2^{(m/2)}-1} P_s. \tag{18}$$

We then discuss the probability $P_2$ of error on the bits modulated in $\overline{d}$ in the case of BPSK and QPSK. For BPSK, the decision is based on the sign of the sum of the two outputs of the correlators for the two sequences detected in the previous step. The case of QPSK is equivalent to two BPSK with half the SNR per each bit, both independently demodulated from the detection of two sequences (the corresponding to subsets $Q_r$ and $Q_i$, respectively). Then, the probability $P_2$ for BPSK and QPSK, respectively, is:

$$P_2 = \frac{1}{2} P_s P_s + 2P_s(1-P_s) Q'_{bpsk} + (1-P_s)(1-P_s) Q_{bpsk}, \tag{19}$$

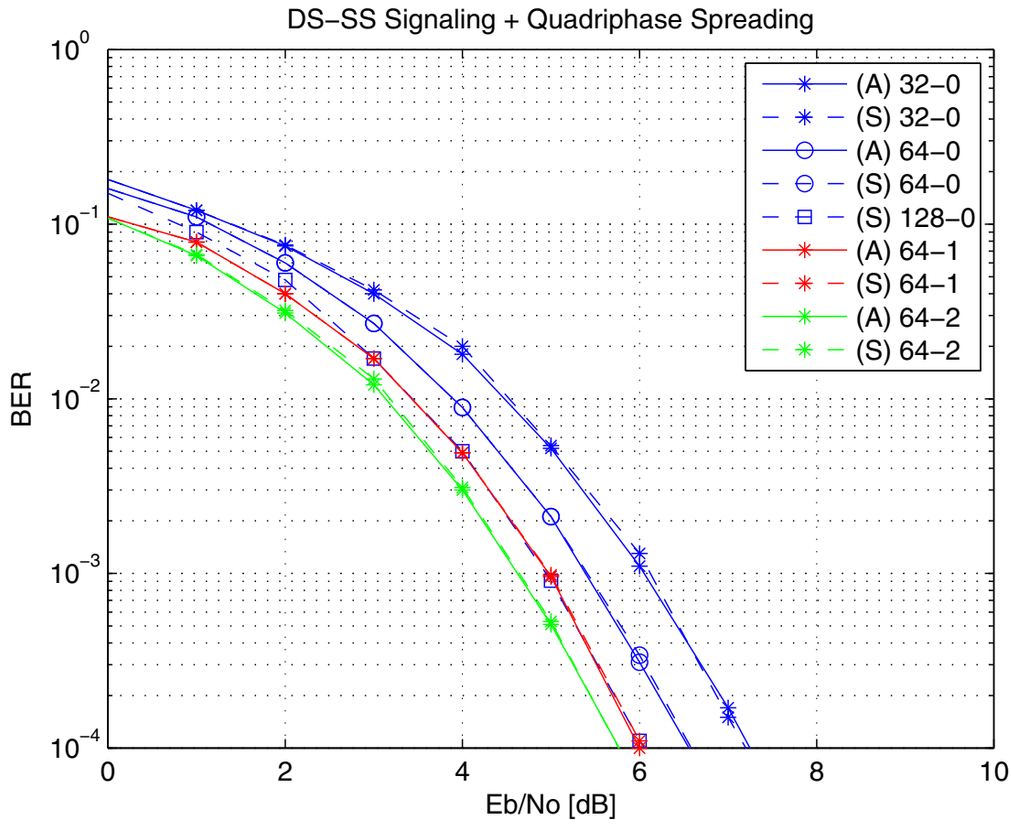


Fig. 2. Probability of error as a function of SNR per bit combining both techniques DS-SS M-ary signaling and quadriphase chip spreading for various values of $M$ (32, 64, 128) and $k$ ($k = 0$ : no modulation, $k = 1$: BPSK, $k = 2$: QPSK). Probability is analytically (A) computed and derived from algorithm simulations (S)

$$P_2 = \frac{1}{2}P_s P_s + P_s(1-P_s)\left(Q'_{bpsk} + 0.5\right) + (1-P_s)(1-P_s)Q'_{bpsk}\,, \tag{20}$$

where

$$Q_{bpsk} = Q\left(\sqrt{2\left(\frac{Eb}{N_o}\right)'}\right) \text{ and } Q'_{bpsk} = Q\left(\sqrt{\left(\frac{E_b}{N_o}\right)'}\right). \tag{21}$$

Finally, the probability $P_b$ of bit error is equal to Equation 14. If we compare Figure 2 with Figure 1 it is shown that, for a given bit-rate, in terms of BER versus SNR per bit (for $k = 0$ with only additive white Gaussian noise) applying DS-SS M-ary signaling using M sequences is almost equivalent to using DS-SS M-ary signaling plus quadriphase chip spreading using $2M$ sequences. In this latter case, however, the process gain is doubled.

When we introduce modulation (i.e. $k \neq 0$) Figure 2 and Figure 1 show that the equivalence noted in the previous paragraph is no longer true: the use of quadriphase chip spreading with sequences of length $2M$ in combination with modulation produces inefficiency in terms of BER with respect to a system that does not use quadriphase chip spreading with sequences of length $M$. This is intuitively explained by noticing that when doubling the length of the

sequence, keeping the same bandwidth, the number of transmitted sequences is halved as is the number of encoded bits in the modulation.

In a symbol time $T_s$, $k+m$ bits are sent ($b_0^{(1)} \cdots b_{k-1}^{(1)} b_0^{(1)} \cdots b_{m-1}^{(1)}$), $k$ bits due to the modulation of $\overline{d}$ and $m$ bits due the choice of the spreading sequence. Therefore, spectral efficiency is:

$$C = \frac{k+m}{G_p} = C_{ss} + \frac{m}{G_p} = C_{ss} + \frac{2\log_2(M/2)}{G_p} \tag{22}$$

Comparing Equation 22 with Equation 15 and equal bit rate, it is shown that quadriphase and biphase chip spreading have an approximate spectral efficiency (assuming $G_p = L \approx M$).

## 3. The experiments

This section describes the outcomes of various experiments based on DS-SS over the link established between the SAS and Spain. Firstly, we define the objectives of the study and point out some methodological criteria that was taken into account. Following, the testbench and the algorithms used to carry out the tests are described. Finally, the experiments are explained and the outcomes derived from them carefully discussed.

### 3.1 Goals

The aim of this work is to experimentally evaluate various alternatives, based on DS-SS, concerning the maximum achievable performance in terms of bit error rate and spectral efficiency at the expense of greater complexity at the receiver side. The final goal is to come up with a proposal for the data transmission link between the SAS and Spain. Therefore, the alternatives that we suggest may combine the following aspects:

- General features: (*i*) frequency chip, (*ii*) modulation.
- Related to DS-SS signaling: (*i*) process gain (determined by $L$), (*ii*) number of bits per sequence (expressed in terms of $M$), (*iii*) spreading: biphase or quadriphase.

However, there are a number of aspects, which are beyond the scope of this study, that must be defined and implemented. They are, specifically: (*i*) frame format, (*ii*) frequency and time synchronization (chip and frame), (*iii*) coding and interleaving and (*iv*) channel estimation and multipath diversity use.

It is noteworthy that it is not the aim of these experiments to measure the percentage of satisfactory receptions among the total number of receptions, since this magnitude is strongly related to the robustness of the synchronization method, which is beyond the scope of this study. Consequently, we will only evaluate expected performance from satisfactory receptions by means of a testbench explained below (see Section 3.3).

Figures 3 and 4 depict a block diagram of the transmitter and receiver, respectively. On one hand, common modules are shown in green. Specifically:

- At transmitter side: (*i*) a binary random source (320 bits), (*ii*) a turbo encoder ($rate = 1/3$) which operates combined with an interleaver (972 coded bits at the output), (*iii*) a frame compiler, designed according to the measured characteristics of multipath and Doppler spread, which builds a frame that consists of: (*iii.a*) a initial field for synchronization and channel estimation, (*iii.b*) a field that is periodically repeated to track channel estimation and (*iii.c*) data (see Section 3.3.1 and Figure 5).

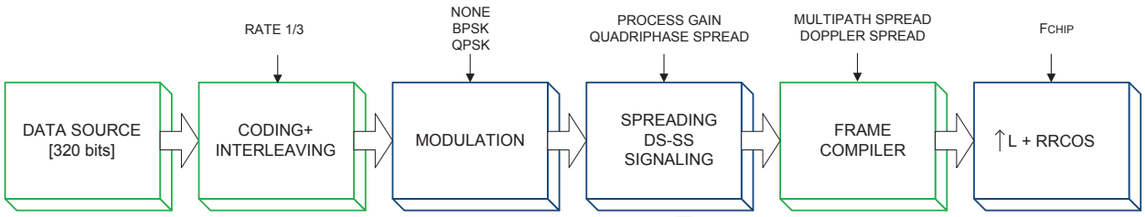


Fig. 3. Transmitter block diagram. Common modules to all experiments (testbench) are shown in green and modules with specific characteristics are shown in blue

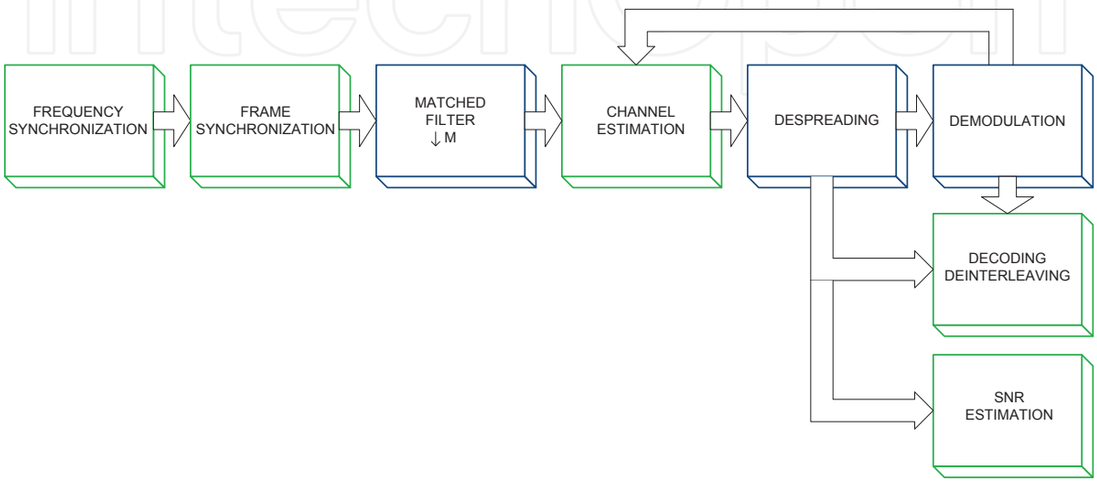


Fig. 4. Receiver block diagram. Common modules to all experiments (testbench) are shown in green and modules with specific characteristics are shown in blue

- At receiver side: (*i*) frequency synchronization by means of an unmodulated tone previously emitted, (*ii*) frame synchronization, (*iii*) channel estimation (*iv*) decoding and deinterleaving and (*v*) a SNR estimation module.

On the other hand, modules with specific parameters for the experiments are shown in blue in both the transmitter and the receiver. These parameters are: (*i*) chip frequency ($f_{chip}$), which determines the signal bandwidth (2500, 3125 and 6250 chips per second), (*ii*) modulation, a choice between no modulation, BPSK or QPSK, (*iii*) the process gain (spreading sequence of length 31, 63 or 127 chips), (*iv*) biphase or quadriphase spreading and (*v*) the number of bits per sequence $\log_2(M)$ (always $L = M - 1$).

### 3.2 Methodology

In this section we explain the approach followed prior to obtaining the outcomes from these experiments. We emphasize the following points:

- According to the explanations of the previous section, all experiments use a common testbench. Consequently, the test algorithms equally affect all experiments.
- Each experiment consists of a signal composed of 320 bits of data (972 coded bits), which are modulated, spread, filtered, and finally appropriate headers are appended to them. This signal has the appearance of a burst with a duration that depends on specific characteristics of the experiment (number of bits per symbol, sequence length,

etc.). Experiments are transmitted during a sounding period that has a maximum time length of 20 seconds, which is repeated every minute except for 18 minutes assigned to maintenance and other functions.

- In each sounding period several signals are transmitted within a frame. Each frame is repeated at least twice within a sounding period (more repetitions will be possible in case of short frames).
- Each sounding period is associated with a carrier frequency. Seven different carrier frequencies have been chosen based on availability outcomes presented in (Vilella et al., 2008). These carrier frequencies are: $\{8078, 8916, 10668, 11411, 12785, 14642, 16130\}$ $[kHz]$. Then, each frequency is tested 6 times per hour.
- Each day consists of 18 available hours (from 18 UTC to 11 UTC, both included).
- Each frame is transmitted a minimum of two days. Under these assumptions, each experiment was performed at a certain time and frequency, at least 24 times (2 days, 6 times per hour, 2 frames per sounding period).
- There are a number of days with frames containing a common experiment. This fact allows the assessment of interday variability.

### 3.3 Testbench

The testbench consists of a frame and a set of algorithms shared between all experiments, which are all described below.

#### 3.3.1 Frame compilation

The testbench is based on a frame which is shown in Figure 5, where:

- **C** is a header based on two identical sequences $\overline{s}$ of length $L^{(s)}$ chips, as follows:

$$\mathbf{C} = \left\{ s_{L^{(s)}-l+1} \cdots s_{L^{(s)}} \, \overline{s} \, \overline{s} \, s_1 \cdots s_l \right\}. \tag{23}$$

  Therefore, **C** has a length of $2L^{(s)} + 2l$ chips, where $l$ is the number of chips circularly added before the first and after the second sequence. This header is used to achieve frame, chip and sample synchronization as well as initial channel estimation. The value of $l$ can be computed by means of the maximum multipath spread of the channel ($\tau_{max}$) as:

$$l = \lceil \tau_{max} f_{chip} \rceil, \tag{24}$$

  where $\lceil \cdot \rceil$ denotes the integer immediately above. Therefore, $l$ is the number of guard chips before and after the block formed by the two sequences $\overline{s}$. This guard ensures both circular correlation during synchronization and channel estimation free from intersymbol interference.
- **S** is a signaling field based on sequence $\overline{s}$, with the following form:

$$\mathbf{S} = \left\{ s_{L^{(s)}-l+1} \cdots s_{L^{(s)}} \, \overline{s} \, s_1 \cdots s_l \right\}. \tag{25}$$

  Therefore, **S** is of length $L^{(s)} + 2l$. The value of $l$ is calculated using Equation 24. This field provides channel estimation tracking. The period of repetition of **S** (denoted by $T_S$) is computed by means of the maximum Doppler spread of the channel ($v_{max}$) as:

$$T_S \approx \frac{1}{10 \, v_{max}}, \tag{26}$$


Fig. 5. Testbench frame format

where the channel is considered to be flat over a tenth of the inverse of $v_{max}$.

- **D** is a data symbol based on a Gold sequence of length $L$ chips. Between the header **C** and the field **S**, or between two consecutive **S** fields there are $B$ symbols that build a block. The number of symbols per block is given by the following equation:

$$B = round\left(\frac{T_S \cdot f_{chip}}{L^{(s)}}\right). \tag{27}$$

#### 3.3.2 Algorithms description

This section explains reception algorithms used by all experiments (in green in block diagram of Figure 4).

Let $r[n]'$ be the signal at the output of a downsampling filter during the sounding period. $r[n]'$ is $\Delta t$ seconds long with $\Delta t \cdot f_m$ samples, where $f_m$ is the sampling frequency at the receiver side ($f_m = 50\,ksps$).

Estimation of frequency synchronization error ($\delta f$) between transmitter and receiver is obtained by applying algorithms explained in (Vilella et al., 2008) to a non modulated signal which is transmitted immediately before the data signal. Then, the signal $r[n]'$ is downconverted to baseband by a complex exponential signal with frequency $-\delta f$:

$$r[n] = r[n]' \cdot e^{2\pi \frac{\delta f}{f_m} n} \tag{28}$$

The next point to be considered is the frame, chip and sample synchronization which is obtained from the header **C** (Alsina et al., 2009). Firstly, emitter and receiver are time synchronized by means of a GPS receiver at each side, with time resolution of one second. Hence, the receiver knows the second $t_a$ in which an experiment is transmitted. Let a synchronization window around $t_a$ : $[t_a - \delta_a/2, t_a + \delta_a/2]$. Then the frame, chip and sample synchronization point $t_s$ is:

$$t_s = \frac{\underset{m}{\text{argmax}}\left(\|S_1\| + \|S_2\|\right)}{f_m},\ m \in [t_a - \delta_a/2, t_a + \delta_a/2] f_m, \tag{29}$$

where

$$S_1 = \sum_{k=0}^{L^{(s)}-1} r[m+k]\overline{s}[k] \text{ and } S_2 = \sum_{k=0}^{L^{(s)}-1} r[m + L^{(s)}\frac{f_m}{f_{chip}} + k]\overline{s}[k], \tag{30}$$

where $\overline{s}$ is the sequence of length $L^{(s)}$, interpolated by a root raised cosine filter, that forms header **C**.

It is noted that $S_1$ and $S_2$ are the correlation of the signal $\overline{r}$ with a replica of the header sequence $\overline{s}$ and with the same header sequence delayed $L^{(s)}$ chips, respectively. Therefore, synchronization probability is maximum for that value of $m$ such that the sequences in $S_1$ and $S_2$ match in phase with header **C**.

It can be easily deduced from Equation 29 and Equations 30 that the greater the length of the sequence $\overline{s}$ (in chips and samples), the greater the likelihood of synchronization; however, the greater the length of the header. So, there is trade-off between synchronization performance and spectral efficiency.

Once frame, chip and sample ($t_s$) are successfully synchronized a matched filter is applied, followed by a decimate process to adjust the signal to one sample per chip (see Figure 4):

$$r_d[k] = \sum_{l=0}^{N_p-1} r[\frac{t_s}{f_m} + k\frac{f_m}{f_{chip}} + l]p[l], \tag{31}$$

where $\overline{p}$ is a pulse of length $N_p$ samples, namely a root raised cosine with roll-off factor $\alpha = 0.65$.

Channel estimation is initally obtained from the second sequence on header **C** and tracked by the field **S** as:

$$h_l = \sum_{k=0}^{L^{(s)}-1} r_d[\frac{\delta t}{f_{chip}} + k + l]s[k],\ l\ in[-\tau_{max}f_{chip}, \tau_{max}f_{chip}], l \in Z, \tag{32}$$

where $\delta t$ denotes the time offset of the sequence (**C** or **S**) from which we obtain channel estimation.

The despreading of each symbol is achieved by a bank of correlators using each of the sequences $\overline{c}^{(m)}$ that belongs to the family denoted by $Q = \{\overline{c}^{(1)}, \overline{c}^{(2)}, \cdots, \overline{c}^{(M)}\}$. The correlation is calculated for all those $l$ values such that the channel estimation exceeds a certain threshold $\gamma$:

$$U^{(m)(l)} = \sum_{k=0}^{L-1} r_d[\frac{t_d}{f_m} + l + k]c^{(m)}[k],\ m \in [1, M],\ \forall l \mid \|h_l\| \geqslant \gamma, \tag{33}$$

where $t_d$ indicates the starting point of the symbol under consideration and $L$ is the length of the sequences used to spread data.

When using quadriphase spreading, the set of sequences $Q$ is divided into two subsets $Q_r = \{\overline{c}^{(1)}, \cdots, \overline{c}^{(M/2)}\}$ on one side and $Q_i = \{\overline{c}^{(M/2+1)}, \cdots, \overline{c}^{(M)}\}$ on the other side. Then we compute both decision variables similarly to Equation 33.

The decision of which sequence has been transmitted is performed based on a criterion of maximum absolute value at the output of the correlators. It is only evaluated over the set or subset of appropriate sequences and for the shift $l$ such that the channel estimation is maximum. We denote by $p$ ($p \in [1, M]$) the index for the sequence with maximum correlator output, when not using quadriphase spreading, and $p_r$ ($p_r \in [1, M/2]$) and $p_i$ ($p_i \in [M/2+1, M]$) when using quadriphase spreading.

The demodulation of bits contained in $\overline{d}$ (see Equation 1) is achieved using a RAKE architecture. If not using quadriphase spreading, the decision is based on the decision variable $U$ computed as follows:

$$U = \sum_l h_l^* \left( U^{(p)(l)} - \sum_{k<l} U^{(p)(k)}\rho^{(p)}(l-k) \right),\ \forall l \mid \|h_l\| \geqslant \gamma, \tag{34}$$

where $\rho^{(p)}$ is the circular autocorrelation of sequence $p$. If applying quadriphase spreading two decision variables ($U_r$ and $U_i$) will be needed, one per each branch.

The value of $p$ (or $p_r$ and $p_i$) determines the bits used by the technique of spread spectrum, and the decision on $U$ (or $U_r$ and $U_i$) determines the bits used by modulation of $\overline{d}$.

If not using quadriphase spreading, each bit mapped to a symbol is linked to a soft-bit $Sb$ that is computed according to the following expression:

$$Sb = \frac{\left\| U^{(p)(l)} \right\|^2}{\frac{1}{M-1} \sum_{m=1, m \neq p}^{M} \left( \| U^{(m)(l)} \mid - \overline{U^{(l)}} \right)^2}, \; l \mid \forall k \neq l, \; \|h_l\| > \|h_k\|, \tag{35}$$

where:

$$\overline{U^{(l)}} = \frac{1}{M-1} \sum_{m=1, m \neq p}^{M} \| U^{(m)(l)} \| . \tag{36}$$

It is noted that the term on the numerator in Equation 35 is a measure of the power of the signal after despreading, while the denominator is an estimation of the noise power, computed at the output of the correlators for those sequences which are not sent. Therefore, the soft-bit is an estimation of the signal to noise ratio after despreading. When using quadriphase spreading, soft-bits are calculated similarly to the biphase spreading option, for both detected sequences ($p_r$ and $p_i$) and the corresponding subsets of sequences ($Q_r$ and $Q_i$).

The noise variance is also computed at the output of the correlators except for those corresponding to the transmitted sequences. Once despreading and demodulation processes have finished (with the corresponding soft-bits) a deinterleaving and a Turbo decoding (Berrou & Glavieux, 1996) are applied. These two modules operate on a set of 972 coded bits and generate a set of 320 decoded bits. The Turbo code has a constraint length of 4 and runs 8 iterations.

If not using quadriphase spreading, SNR estimation is obtained averaging soft-bits values for each symbol of the burst. Specifically:

$$SNR = \frac{1}{N_{symbols}} \sum_{n=0}^{N_{symbols}-1} \frac{Sb^{(n)}}{L}. \tag{37}$$

### 3.4 Outcomes

As a summary of the characteristics of most of the experiments carried out during the Antarctic season 2006/07 we have compiled Table 1. For each configuration we give the bandwidth ($f_{chip}$), the length of the sequence ($L$), the number of sequences ($M$), the use of quadriphase (QS), the type of modulation, the achieved bit rate, the spectral efficiency ($C$) (in parenthesis) and finally, the number of days each experiment was transmitted.

In order to summarize the outcomes obtained from the experiments carried out on the link between the SAS and Spain the plots shown in Figures 6 and 7 contain information from tens of thousands of bursts and are compared to the maximum achievable performance discussed in Section 2.4.

| Config. | $f_{chip}$ | $L$ | $M$ | QS | Modulation | bit rate ($C$) | | Num. days |
|---|---|---|---|---|---|---|---|---|
| | | | | | | uncoded | coded | |
| (1) | 2500 | 63 | 64 | 0 | none | 238 (0.10) | 79 (0.03) | 1 |
| (2) | 2500 | 63 | 64 | 1 | none | 397 (0.16) | 132 (0.05) | 1 |
| (3) | 2500 | 63 | 64 | 1 | QPSK | 476 (0.19) | 159 (0.06) | 4 |
| (4) | 2500 | 31 | 32 | 1 | QPSK | 806 (0.32) | 267 (0.11) | 2 |
| (5) | 3125 | 63 | 64 | 0 | none | 298 (0.10) | 99 (0.03) | 1 |
| (6) | 3125 | 63 | 64 | 1 | none | 496 (0.16) | 165 (0.05) | 1 |
| (7) | 3125 | 63 | 64 | 1 | QPSK | 595 (0.19) | 198 (0.06) | 11 |
| (8) | 3125 | 31 | 32 | 1 | QPSK | 1008 (0.32) | 336 (0.11) | 2 |
| (9) | 6250 | 63 | 64 | 0 | none | 595 (0.10) | 198 (0.03) | 1 |
| (10) | 6250 | 63 | 64 | 1 | none | 992 (0.16) | 331 (0.05) | 1 |
| (11) | 6250 | 63 | 64 | 1 | QPSK | 1190 (0.19) | 397 (0.06) | 5 |

Table 1. Configurations of the experiments carried out on the ionospheric link between the SAS and Spain during the 2006/07 Antarctic season

The basic plot that is used to show the most important outcomes is a scatterplot (see, for instance, the two top pictures in Figure 6 containing $BER^{(')}$ performance versus SNR estimation. The estimation of SNR at the receiver side is computed immediately after despreading by means of Equation 37. Regarding this estimation it should be noted that (*i*) the signal strength is measured by means of only the most powerful path and hence, the signal at the receiver input is actually higher in case of multipath channel, (*ii*) when the detector at the output of correlators commits an error the subsequential SNR estimation is incorrect (see, for instance, Figure 6 (top) which shows that the detector systematically fails, producing $BER^{(')}$ close to 0.5 when the SNR is approximately -8 dB).

$BER^{(')}$ refers to the bit error rate measured on bits contained in a burst of $N_{bits}$ (320 uncoded bits). Therefore, each point (SNR,$BER^{(')}$) of the scatterplot corresponds to the demodulation of a burst of $N_{bits}$. The thick line shown on each scatterplot is obtained by calculating the median of points of $BER^{(')}$ in consecutive subintervals of width 0.02.

The relationship between BER and SNR can be obtained by simulation, or analytically, according to the explanations in Section 2.4. Then, the probability $P$ that a burst of $N_{bits}$ contains $k$ erroneous bits is:

$$\mathrm{P}\left(\mathrm{BER}^{(')} = \frac{k}{N_{bits}}\right) = \binom{N_{bits}}{k} \mathrm{BER}^{k} \left(1 - \mathrm{BER}\right)^{N_{bits}-k}. \tag{38}$$

We define the interval $\left[BER_l^{(')}, BER_h^{(')}\right]$ which, given a BER, contains with a probability of 90 % a defined $BER^{(')}$. Specifically:

$$\mathrm{P}\left(\mathrm{BER}^{(')} < \mathrm{BER}_l^{(')}\right) = 0.05 \text{ and } \mathrm{P}\left(\mathrm{BER}^{(')} > \mathrm{BER}_h^{(')}\right) = 0.05\,. \tag{39}$$

These scatterplots includes $BER_l^{(')} = f(SNR)$ and $BER_h^{(')} = f(SNR)$ curves for the analogous configuration. All the points should be found in 90 % of cases in the space between these curves if the tests were performed in a laboratory in the presence of only additive white Gaussian noise. However, as shown in Figures 6 and 7, it should be noted that in all scatterplots points are located outside the space bounded by the curves $BER_l^{(')}$ and $BER_h^{(')}$ and shifted about 2 dB to higher SNRs. This shift is due to different causes: (*i*) interference and no Gaussian noise, (*ii*) channel: multipath, Doppler, fading, etc., (*iii*) etc. The optimization of testbench algorithms could mitigate this loss of performance, but in any case we must take into account this shift when performing the design from a theoretical point of view.

Each scatterplot is accompanied by two histograms which derive from it. The first of these histograms shows, for each SNR, the percentage of receptions with $BER^{(')} = 0$ of the total number of receptions $BER^{(')} = 0$. It is noted that the higher the SNR the higher the probability of demodulating with $BER^{(')} = 0$, but simultaneously that SNR is less likely. This first histogram shows, therefore, the values of SNR at which the experiment is more successful. The second histogram shows, for each SNR, the percentage of receptions with $BER^{(')} = 0$ of the total number of receptions at that SNR. This figure allows us to evaluate at which SNR the probability of receiving a burst without errors is above a given value.

The results are discussed in terms of comparison with expected theoretical values. Specifically, in Figure 6 a scatterplot shows the effect of the variation in bandwidth and in Figure 7 the use of modulation is studied. Furthermore, in Figure 8 frequencies with best percentage of receptions of bursts with $BER^{(')} = 0$ per hour are shown and in Figure 9 the hours with best percentage of receptions of bursts with $BER^{(')} = 0$ at each frequency are also shown.

#### 3.4.1 Bandwidth

Figure 6 compares the use of configuration (L, M, QS, Mod): (63, 64, yes, QPSK) with coded bits using a bandwidth of 3125 Hz (left column) and the same configuration using a bandwidth of 6250 Hz (right column). It is observed that the benefits obtained are slightly better for high bandwidth: for instance for SNR= -6 dB about 25 % of the receptions are $BER^{(')} = 0$ when $f_{chip}$= 3125 Hz, whereas this amount is over 40 % when $f_{chip}$ = 6250 Hz (the percentages are also better in the second case for higher SNRs: -5 dB, -4 dB, -3 dB, etc.). This fact may be partly explained by a better performance of the RAKE receiver when working with higher multipath resolution.

#### 3.4.2 Modulation

Figure 7 compares the application of QPSK modulation with a configuration with no modulation based on a system with (L, M, QS): (63, 64, yes) with coded bits and a bandwidth of 3125 Hz. Curves $BER_l^{(')}$ and $BER_h^{(')}$ indicate that theoretical maximum benefits are almost identical (slightly better when not using any modulation). The histograms confirm this estimation, where small deviations of about 5 % or 10 % to the no modulation option are observed.

It is worth noting that when using modulation the channel must be estimated and the use of a RAKE module is advised. Therefore, computational complexity is slightly increased while

spectral efficiency improves without additional energy cost. In this context, we highlight the fact that the results of degradation of 2 dB observed between theory and experimental outcomes appear in both cases: modulation and no modulation. Therefore, this malfunction can be attributed to detection algorithms rather than the channel estimator and combiner algorithms.

### 3.4.3 Best frequencies

Figure 8 shows frequencies with best $BER^{(')}$ percentage, based on configuration (L, M, QS, Mod): (63, 64, yes, QPSK) with coded bits and a bandwidth of 3125 Hz. It should be noted that this configuration experimentally obtained $BER^{(')} = 0$ for SNR above -6 dB with probability greater than 80 % (see Figure 7). If we compare this figure with frequency availability results presented in (Vilella et al., 2008), which indicates the frequency with highest availability at a given SNR in a 3 kHz bandwidth, we can highlight that: $(a)$ The distribution of frequencies with best availability rates is very similar in both studies: above 15 MHz between 18 and 22 UTC, from 9 MHz to 11 MHz between 23 and 6 UTC, and again about 15 MHz between 7 and 11 UTC. Therefore, there is a very good correspondence between channel sounding results and the analysis of data transmissions. $(b)$ If we focus on specific values of percentages, we observe that ($b.i$) there are a set of hours, mostly belonging to the evening and morning (20, 21, 23, 2, 5, 6, 7, 8, 10 UTC) when the probability of overcoming -3 dB (measured by channel sounding) coincides, with high accuracy, with the probability of obtaining $BER^{(')} = 0$ (measured by data analysis). ($b.ii$) There are a number of hours at night (0, 1, 3, 4 UTC) when the probability of obtaining $BER^{(')} = 0$ is approximately 45 % below the prediction made by narrow-band sounding. ($b.iii$) Finally, a set of hours in both measures show mixed results (18, 22, 9 UTC). 18 and 9 UTC are noteworthy because the channel study shows very low availability (less than 5 %), whereas data analysis gets $BER^{(')} = 0$ with rates around 20%.

One possible explanation for these results could be derived from the following two arguments: ($i$) SNR measurements conducted by channel sounding consider noise everything that is not the transmitted signal (Gaussian noise and interference). During evening (18 to 22 UTC) and morning (07 to 11 UTC) the weight of interference power with respect to the total noise power is lower than during full night (23 to 06 UTC). It is precisely in the evening and morning when the two measurements (channel and data) are more similar. From this statement we can conclude that, rather than Gaussian noise, interference is the main factor on signal degradation. ($ii$) At full night and low frequencies (6 MHz to 10 MHz) channel time dispersion is greater than during evening and morning at high frequencies (14 MHz to 16 MHz) and, therefore, it is more difficult to obtain good performance for the same SNR (Vilella et al., 2008).

### 3.4.4 Best hours

Figure 9 shows the hours with highest percentage of $BER^{(')} = 0$ at each frequency, based on the configuration (L, M, QS, Mod): (63, 64, yes, QPSK) with coded bits and a bandwidth of 3125 Hz. This plot is especially useful when trying to use a directive antenna tuned to a particular frequency. It is found that the best results are achieved at high frequencies (around 16 MHz) in the early hours of night (21 UTC).

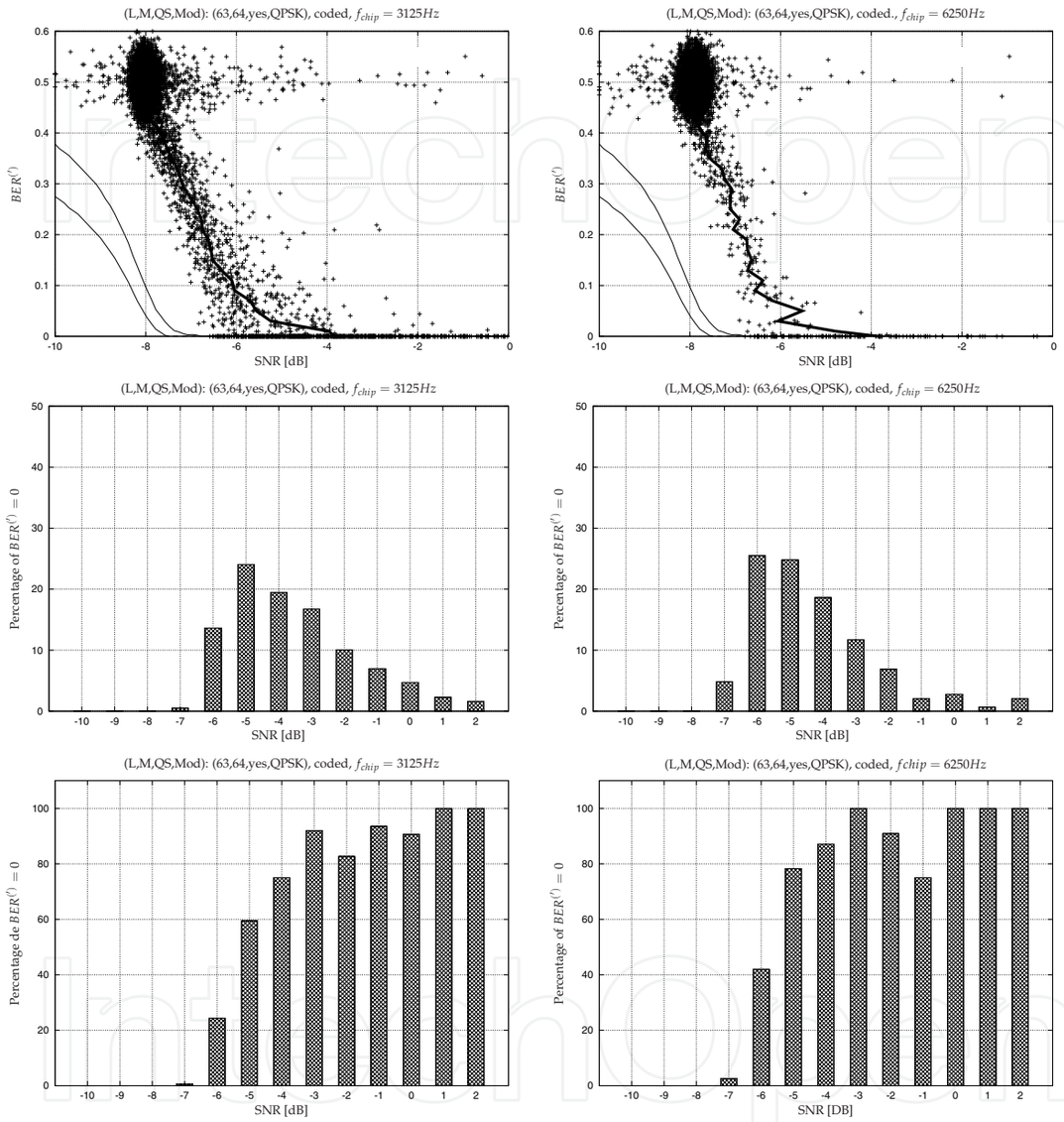


Fig. 6. Comparison of bandwidths (3125 Hz and 6250 Hz): (*i*) Scatterplot of $BER^{(')}$ versus SNR estimation before despreading (top row), (*ii*) histogram of the percentage of receptions with $BER^{(')} = 0$ to total receptions with $BER^{(')} = 0$ (middle row); (*iii*) histogram of the percentage of receptions with $BER^{(')} = 0$ to total receptions at that SNR (bottom row). The curves $BER_l^{(')}$ and $BER_h^{(')}$ are included on the scatterplots

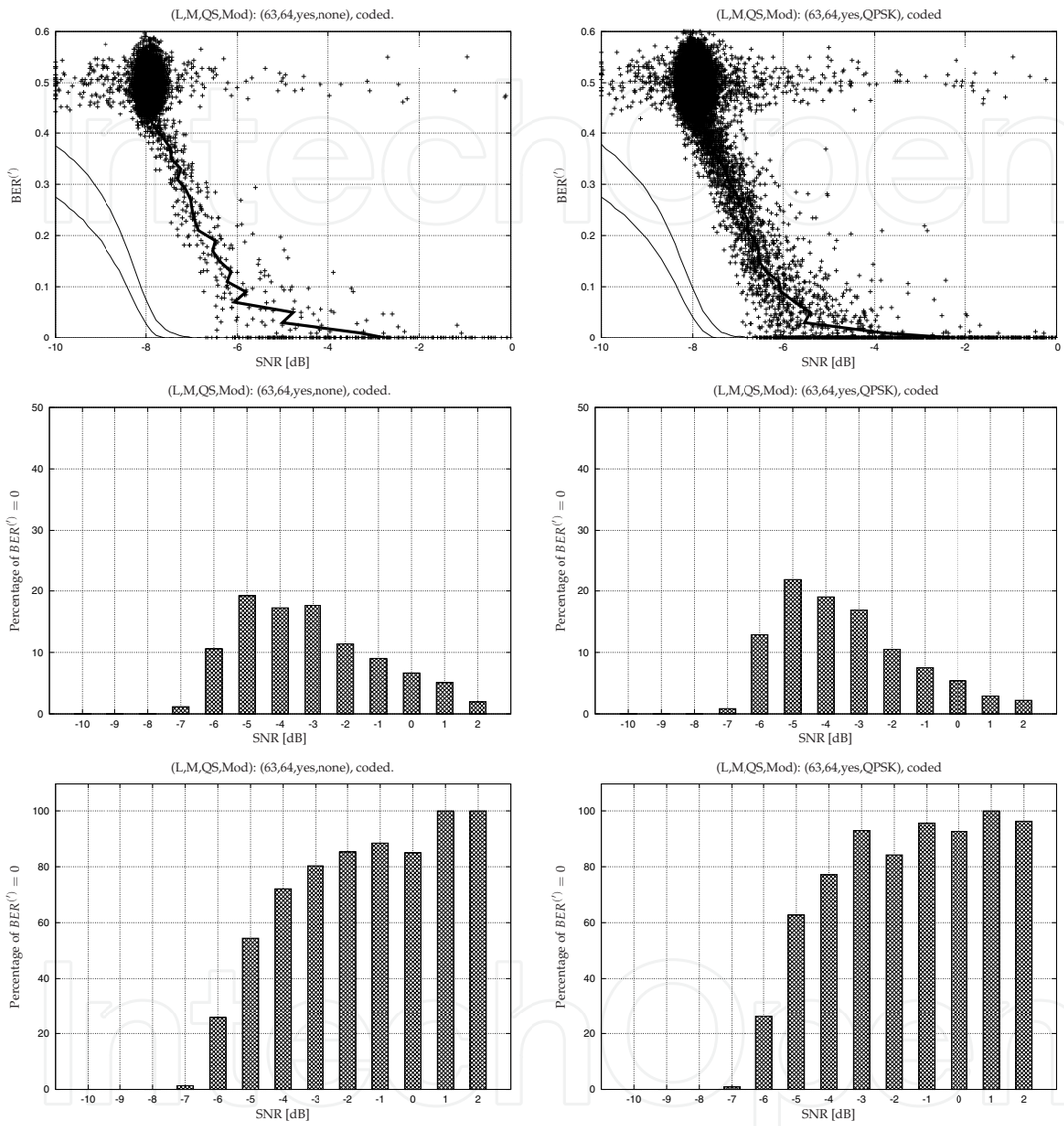


Fig. 7. Comparison of modulation (none and QPSK): (*i*) Scatterplot of $BER^{(')}$ versus SNR estimation before despreading (top row), (*ii*) histogram of the percentage of receptions with $BER^{(')} = 0$ to total receptions with $BER^{(')} = 0$ (middle row); (*iii*) histogram of the percentage of receptions with $BER^{(')} = 0$ to total measurements at that SNR (bottom row). The curves $BER_l^{(')}$ and $BER_h^{(')}$ are included on the scatterplots

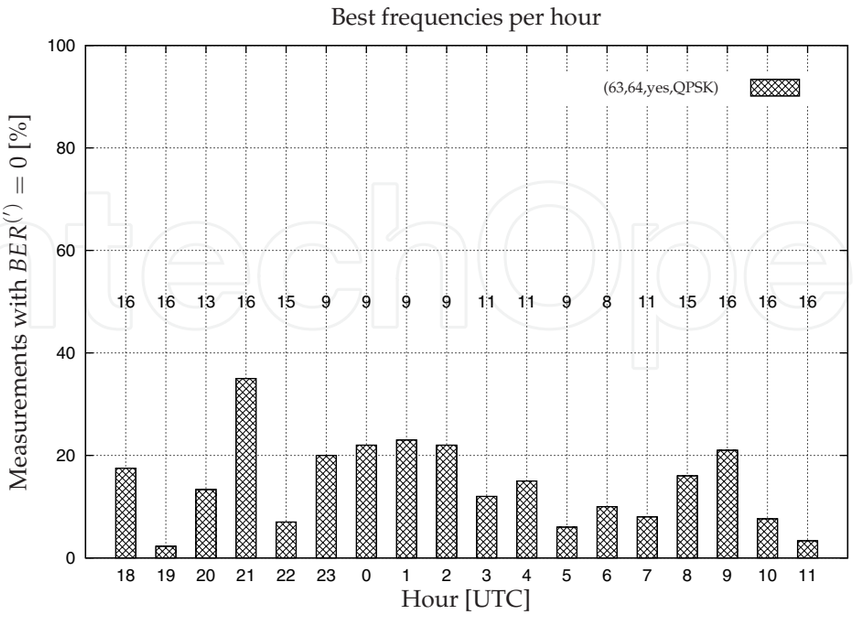


Fig. 8. Frequencies [MHz] with highest percentage of measurements with $BER^{(\prime)} = 0$ per hour. The plot is based on the following configuration (L, M, QS, Mod): (63, 64, yes, QPSK) with channel coding

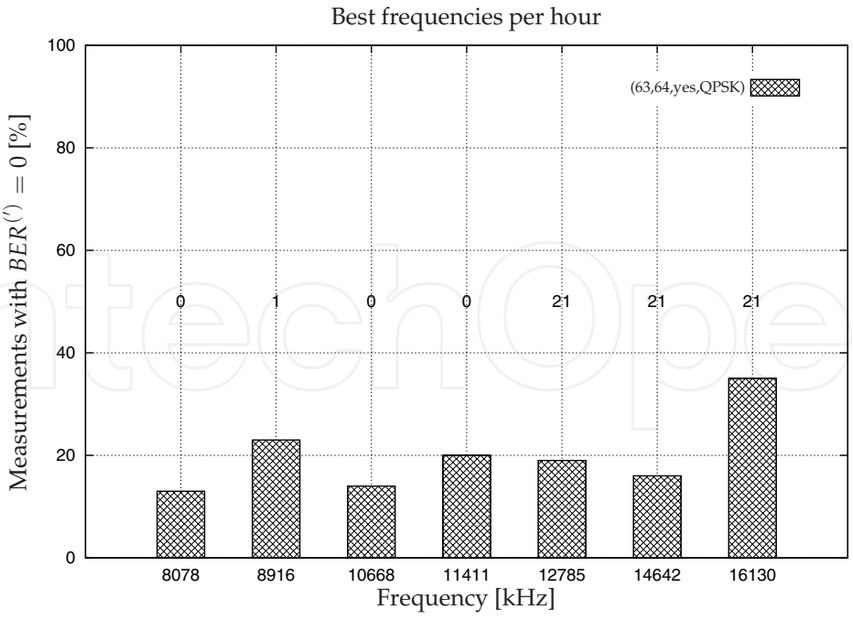


Fig. 9. Hours [UTC] with highest percentage of measurements with $BER^{(\prime)} = 0$ at each carrier frequency. The plot is based on the following configuration (L, M, QS, Mod): (63, 64, yes, QPSK) with channel coding

## 4. Conclusions

Throughout this chapter we have studied, both theoretically and experimentally, the feasibility of low rate data transmission over a very long ionospheric link. The ionosphere may be used as a communications channel available from anywhere on the Earth. Hence it can be adopted as a solution to cope with deficient or non-existent satellite coverage range. We have focused our research work on the link between the Spanish Antarctic Base Juan Carlos I and Spain. It has a length of approximately 12700 km along the surface of the Earth and passes over 4 continents in a straight line. The system is currently applied to the transmission of data of a geomagnetic sensor that generates a maximum of 5120 bits per day. The special conditions found in Antarctica have impaired several aspects of the transmission. To conserve energy, maximum transmit power is set at 250 watts. In addition, to prevent further environmental impact, a non directive antenna (a monopole) requiring minimal infrastructure and installation was chosen to be placed at the SAS.

We have reviewed current HF communication standards and noted that none of them are intended for links with negative SNR. Thus we propose a novel system to be used on the physical layer of a ionospheric link based on a Direct Sequence Spread Spectrum technique. The determining factors for the use of this technique were its robustness to multipath and narrowband interference, its ability to transmit with low power spectral density, and its flexibility in terms of spectral efficiency in scenarios with negative SNR.

We propose a mode of transmission outside of current ITU standards, designed to cause minimal interference to primary and secondary services defined by the official agencies, able to operate in the presence of high values of noise power and interference, and robust to time and frequency channel dispersion. Hence, we suggest a transmission system based on sporadic short bursts of low density spectral power, focusing on increasing spectral efficiency and energy savings at the expense of a higher complexity receiver.

Several variants of DS-SS have been evaluated: signaling waveform, quadrature spreading and the impact of the modulation (BPSK and QPSK), all of them from the point of view of BER versus SNR per bit and spectral efficiency. We then conclude that:

- The DS-SS M-ary signaling technique allows an increase in spectral efficiency. The higher the number of sequences ($M$) the lower the SNR per bit required to achieve a given BER. In practice, if we use Gold spreading sequences, the maximum value of $M$ is limited by the length of the spreading sequences ($M \sim L$). However, for a given bit-rate, if we increase $M$, the computational complexity at the receiver side increases.
- The combined use of modulation (BPSK and QPSK) and DS-SS M-ary signaling reduces the minimum required SNR per bit to achieve a certain BER. A greater reduction can be achieved with QPSK than with BPSK. However, modulation techniques require channel estimation (except for differential modulation) and, optionally, a RAKE combiner.
- If we add quadriphase spreading to DS-SS M-ary signaling (without modulation), gain can be doubled while maintaining BER and spectral efficiency performance. When using modulation, the use of quadriphase spreading results in energy inefficiency.

We assessed the suitability of studying a channel code based on the use of a Turbo code (rate $= 1/3$), with inner interleaver, that converts a burst of 320 bits into 972 coded bits. Simulations (not shown here for reasons of brevity) demonstrate that coding gain is only achieved for BER

values below $10^{-4}$. The reasons for using coding techniques will therefore depend, among other factors, on the size of the burst of bits and on the desired probability of error free.

We have defined a testbench to experimentally evaluate various configurations and to compare experiment outcomes with theoretical predictions. The testbench includes: (*i*) the definition of a header adapted to time and frequency channel dispersion to perform synchronization and channel estimation, (*ii*) the definition of a data frame, (*iii*) the design of a set of algorithms: encoding/decoding, synchronization, spreading/despreading, RAKE combiner, demodulator and SNR estimation.

The outcomes gathered from this testbench have shown that, for instance, with a SNR of -5 dB, this ionospheric data transmitter is able to transmit data (6 kHz and 320 bits burst size) with a rate of 397 bits per second (error free) with a successful probability of approximately 95 % (see Table 1 and Figure 6). It is noted that this rate would suffice to send the amount of data required by the application (5120 bits per hour), with sporadic frequency transmissions.

Experimental tests have been performed for different configurations and at different bandwidths in a frequency range between 8 MHz and 16 MHz and a time interval between 18 and 12 UTC. From the experimental results and comparison, with theoretical predictions in terms of BER versus SNR, the following conclusions can be drawn:

- There is a loss of about 2 dB of SNR between the theoretical and experimental BER. This loss may be attributable to several factors: non-Gaussian noise, interference, channel dispersion, and so on.
- For a given SNR, the probability of receiving a burst without error is slightly higher for higher bandwidths. This improvement may be due to better performance of the RAKE combiner due to higher multipath resolution (this result should be confirmed in later experiments).
- Experimental results confirm that for a given SNR at the receiver, the use of modulation added to signaling techniques (thus increasing the bitrate without increasing the transmitted power) does not affect the BER performance.
- Regarding the frequencies that are more likely to transmit error free bursts, we observe that they correspond with great accuracy to those with highest availability, measured by channel studies ((Vilella et al., 2008)): above 15 MHz in the evening (18 to 22 UTC) and morning (7 to 11 UTC), and below 11 MHz in the early morning (23 to 6 UTC). Regarding specific percentages of bursts without errors, it appears that they are very similar to those equivalent measurements done by channel studies during the evening and morning, but are worse at night and early morning. This is mainly attributed to the increased amount of interference at night.

According to experimental results we make the following recommendations: (*i*) integrate the loss of 2 dB of SNR into theoretical calculations, (*ii*) prioritize larger bandwidths, use modulation (QPSK rather than BPSK) and use coding techniques, (*iii*) use modulation plus M-ary signaling without quadriphase spreading, (*iv*) optimally attempt to establish the data link at 21 UTC (at 16 MHz), or from 23 to 6 UTC (within the range 9-11 MHz).

## 5. Acknowledgments

This work has been funded by the Spanish Government under the projects REN2003-08376-C02-02, CGL2006-12437-C02-01/ANT, CTM2008-03236-E/ANT,

CTM2009-13843-C02-02 and CTM2010-21312-C03-03. La Salle thanks the *Comissionat per a Universitats i Recerca del DIUE de la Generalitat de Catalunya* for their support under the grant 2009SGR459. We must also acknowledge the support of the scientists of the Observatory de l'Ebre throughout the research work.

## 6. References

Alsina, R. M., Bergada, P., Socoró, J. C. & Deumal, M. (2009). Multiresolutive Acquisition Technique for DS-SS Long-Haul HF Data Link, *Proceedings of the 11th Conference on Ionospheric Radio Systems and Techniques*, IET, Edimburgh, United Kingdom.

Bergada, P., Deumal, M., Vilella, C., Regué, J. R., Altadill, D. & Marsal, S. (2009). Remote Sensing and Skywave Digital Communication from Antarctica, *Sensors* 9(12): 10136–10157.

Berrou, C. & Glavieux, A. (1996). Near optimum error correcting coding and decoding: Turbo-codes, *IEEE Transactions on Communications* 44(10): 1261–1271.

Deumal, M., Vilella, C., Socoró, J. C., Alsina, R. M. & Pijoan, J. L. (2006). A DS-SS Signaling Base System Proposal for Low SNR HF Digital Communications, *Proceedings of the 10th Conference on Ionospheric Radio Systems and Techniques*, IET, London, United Kingdom.

Enge, P. K. & Sarwate, D. V. (1987). Spread-spectrum multiple-access performance of orthogonal codes: Linear receivers, *IEEE Transactions on Communications* 35(12): 1309–1319.

IEEE802.11 (2007). *Wireless LAN Medium Access Control (MAC) and Physical Layer (PHY) - Specifications (2007 Revision)*, number doi:10.1109/IEEESTD.2007.373646.

MIL-STD-188-110A (1991). *Interoperability and Performance Standards for Data Modems*, U.S. Department of Defense.

MIL-STD-188-110B (2000). *Interoperability and Performance Standards for Data Modems*, U.S. Department of Defense.

MIL-STD-188-141A (1991). *Interoperability and Performance Standards for Medium and High Frequency Radio Equipment*, U.S. Department of Defense.

Milstein, L. B. (1988). Interference rejection techniques in spread spectrum communications, *IEEE Transactions on Communications* 76(6): 657–671.

NTIA (1998). High frequency radio automatic link establishment (ALE) application handbook, *NTIA handbook*.

Peterson, R. L., Ziemer, R. E. & Borth, D. E. (1995). *Introduction to Spread Spectrum Communications*, Prentice Hall.

Pickholtz, R. L., Schilling, D. L. & Milstein, L. B. (1982). Theory of spread-spectrum communications - a tutorial, *IEEE Transactions on Communications* 30(5): 855–884.

Proakis, J. G. (1995). *Digital Communications*, McGraw-Hill.

Schilling, D. L., Milstein, L. B., Pickholtz, R. L. & Brown, R. W. (1980). Optimization of the processing gain of an M-ary direct sequence spread spectrum communication system, *IEEE Transactions on Communications* 28(8): 1389–1398.

Solé, J. G., Alberca, L. F. & Altadill, D. (2006). Ionospheric Station at the Spanish Antarctic Base: Preliminary Results (in Spanish), *Proceedings of the 5th Asamblea Hispano-Portuguesa de Geodesia y Geofísica*, Sevilla, Spain.

STANAG-4406 (1999). *Military Message Handling System (MMHS)*, North Atlantic Treaty Organization.

STANAG-5066 (2000). *Profile for High Frequency (HF) Radio Data Communications*, North Atlantic Treaty Organization.

Third Generation Partnership Project (1999). *Physical layer - General description Release'99*, number 3GPP TS 25.201, Technical Specification Group Radio Access Network.

Vilella, C., Miralles, D., Altadill, D., Costa, F., Solé, J. G., Torta, J. M. & Pijoan, J. L. (2009). Vertical and Oblique Ionospheric Soundings over a Very Long Multihop HF Radio Link from Polar to Midlatitudes: Results and Relationships, *Radio Sci.* 44(doi:10.1029/2008RS004001).

Vilella, C., Miralles, D. & Pijoan, J. L. (2008). An Antarctica-to-Spain HF ionospheric radio link: Sounding results, *Radio Sci.* 43(doi:10.1029/2007RS003812).

Viterbi, A. J. (1995). *CDMA: Principles of Spread Spectrum Communication*, Prentice Hall PTR.

Zuccheretti, E., Tutone, G., Sciacca, U., Bianchi, C. & Arokiasamy, B. (2003). Vertical and oblique ionospheric soundings over a very long multihop hf radio link from polar to midlatitudes: Results and relationships, *Ann. Geophys* (46): 647–659.

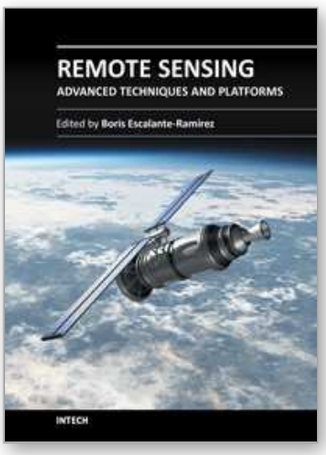


**Remote Sensing - Advanced Techniques and Platforms**
Edited by Dr. Boris Escalante

ISBN 978-953-51-0652-4
Hard cover, 462 pages
**Publisher** InTech
**Published online** 13, June, 2012
**Published in print edition** June, 2012

This dual conception of remote sensing brought us to the idea of preparing two different books; in addition to the first book which displays recent advances in remote sensing applications, this book is devoted to new techniques for data processing, sensors and platforms. We do not intend this book to cover all aspects of remote sensing techniques and platforms, since it would be an impossible task for a single volume. Instead, we have collected a number of high-quality, original and representative contributions in those areas.



INTECH
open science | open minds

**InTech Europe**
University Campus STeP Ri
Slavka Krautzeka 83/A
51000 Rijeka, Croatia
Phone: +385 (51) 770 447
Fax: +385 (51) 686 166
www.intechopen.com

**InTech China**
Unit 405, Office Block, Hotel Equatorial Shanghai
No.65, Yan An Road (West), Shanghai, 200040, China
中国上海市延安西路65号上海国际贵都大饭店办公楼405单元
Phone: +86-21-62489820
Fax: +86-21-62489821

IntechOpen